PCCP

ARTICLE

Gas Phase RDX Decomposition Pathways using Coupled Cluster Theory

Robert W. Molt, Jr.[a,c], Thomas Watson, Jr.[b], Alexandre P. Bazanté[b], Rodney J. Bartlett[b] and Nigel G. J. Richards[c]

Electronic and free energy barriers for a series of gas-phase RDX decomposition mechanisms have been obtain using coupled cluster singles, doubles, and perturbative triples with complete basis set (CCSD(T)/CBS) electronic energies for MBPT(2)/cc-pVTZ structures. Importantly, we have located a well-defined transition state for NN homolysis, in the initial RDX decomposition step, thereby obtaining a true barrier for this reaction. These calculations support the view that HONO elimination is preferred at STP over other proposed mechanisms, including NN homolysis, "triple whammy" and NONO isomerization. Indeed, our calculated values of Arrhenius parameters are in agreement with experimental findings for gas phase RDX decomposition. We also investigate a number of new pathways leading to breakdown of the intermediate formed by the initial HONO elimination, and find that NN homolysis in this intermediate has an activation energy barrier comparable with that computed for HONO elimination.

Introduction

RDX (Fig. 1) is the main component of C4 explosive, and functionalized derivatives are the basis of related modern explosives like HMX and CL-20. The decomposition mechanism of RDX in the various phases has been studied for about 70 years. A large number of details remain obscure, however, because of technical difficulties in both the interpretation of experimental data and the application of computational methods. For example, Brill *et al.*[1] noted that estimates of the activation energy for decomposition covered a large range of values.

As might be anticipated, there is a vast literature on the structure,[2–11] spectroscopic properties[6,12,13] and chemistry of RDX and related nitramines.[2,14–22] Experimental and computational studies have led to a plethora of possible mechanisms for the pathways by which RDX might decompose (Fig. 1),[23] with the situation being complicated by arguments about whether this chemical reaction takes place in the gas, liquid or solid. For example, the high vapour pressure of the solid led Cosgrove and Owens[24] to argue that RDX decomposition begins solely in the gas phase, and early measurements by Robertson[25] suggested that gas phase decomposition has an activation energy of 47 ± 2 kcal/mol and exhibits first-order kinetics. A similar value for the activation energy barrier of 49 kcal/mol was reported by Rauch and Fanelli[26] who also found that the gas-phase mechanism produces NO_2, presumably via homolysis of the N-N bond (Fig. 1A). Subsequent work by Rogers and Daub,[27] however, gave a very different gas phase barrier of 34.1 kcal/mol and it was argued that other decomposition mechanisms could take place. Evidence for one such mechanism was provided by pulsed-laser spectroscopy,[28] which suggested that the transition state for decomposition involved a 5-membered ring, consistent with the concerted elimination of HONO (Fig. 1b). This proposal was also consistent with the observation of a primary KIE for RDX decomposition in the solid phase by Bulusu *et al.*[29] At about the same time, infrared multi-photon dissociation studies led Lee, Hintsa and Zhao to propose yet another alternative: the so-called "triple whammy" mechanism (Fig. 1C), in which decomposition takes place via concerted "depolymerisation" of the RDX molecule.[30] To add to the confusion, Im *et al*. subsequently proposed that one of the NNO_2 groups in RDX isomerizes to form an "NONO isomer" (Fig. 1D) on the basis of electronic spectroscopy, which showed that a vibrationally "hot" but rotationally "cold" NO molecule was formed as an initial decomposition product. They also argued that HONO elimination does not take place in the gas phase because they did not detect its characteristic electronic signature.[31]

In principle, computational studies offer a chance to resolve exactly what decomposition pathways take place in the gas-phase and the extent to which different mechanisms take

[a] *Department of Chemistry and Chemical Biology, Indiana University-Purdue University Indianapolis, Indianapolis, IN 46202, United States*
[b] *Quantum Theory Project, University of Florida, Gainesville, FL 32611, United States*
[c] *School of Chemistry, Cardiff University, Park Place, Cardiff, CF10 3AT, United Kingdom*

† Electronic Supplementary Information (ESI) available: Post NN homolysis reaction pathways, reaction energies, Cartesian coordinates of all structures and reference SCF wavefunctions used in MBPT(2) geometry optimizations.
See DOI: 10.1039/x0xx00000x

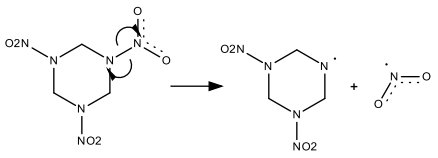

a.) N-N homolysis mechanism; supported by N isotope scrambling experiments[32]

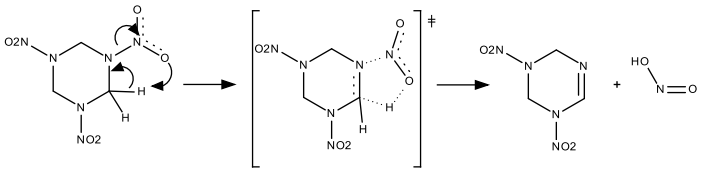

b: HONO elimination mechanism; kinetic isotope effects support involvement of hydrogen in the rate-limiting step[33]

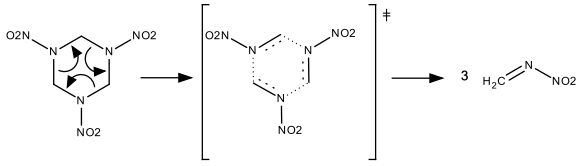

c: "Triple whammy" mechanism[30]

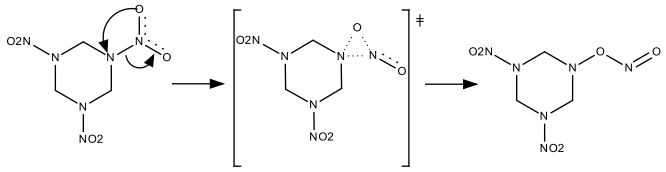

d: NONO isomerization; supported by the observation of vibrationally hot, rotationally cold NO molecules[31,34,35]

Fig. 1: Four hypothetical mechanisms for the initial decomposition step of RDX in the gas phase.

place simultaneously. The situation is complicated, however, by the fact that calculated energy differences for given mechanisms[36–39] can often be smaller than the accuracy of the computational methods used to obtain them; higher resolution QM methods are therefore of value if this problem is to be addressed. The CCSD(T) method[40,41] achieves greater than 1.0 kcal/mol accuracy on single-reference wavefunction molecules when used with a triple-zeta basis set for enthalpies.[42] Although traditionally limited to calculations on relatively few heavy atoms, successful efforts to implement coupled cluster theory in a highly parallel manner[43] now make it possible to apply this approach in studies of systems as large as RDX. We therefore report new calculations on possible RDX decomposition mechanisms, which employ coupled cluster singles, doubles, and perturbative triples (CCSD(T)) with complete basis set (CBS) extrapolation. This approach has the proven ability to provide reaction energy barriers that are sufficiently accurate for use in teasing apart the possible decomposition pathways of RDX.[40,44–47] Not only do our studies build on previous computational efforts by Chakraborty *et. al.*[38] and Miao *et al.*[39] to a more accurate degree, but they have also permitted us to locate the transition state for N-N bond homolysis and delineate the kinetic barriers to subsequent reactions following the initial step.

Computational Methodology

For all structures discussed herein, we used second order many-body perturbation theory, MBPT(2)[48]/cc-pVTZ calculations for geometry optimizations (accurate, on average, to within 0.01 Å for geometries of single-reference molecules),[49] normal mode analysis, and the evaluation of partition functions for free energy estimates. MBPT(2) is also known as MP2 when a canonical Hartree-Fock reference is used in the calculation, which was the case here for all closed shell species. All calculations were performed using analytical gradients and second derivatives, increasing the accuracy of partition function contributions arising from small vibrational modes within the harmonic oscillator approximation. For radical species, the UHF wavefunction could not be converged in some cases during geometry optimization, and we had to rely on ROHF strategies (all other cases employed UHF calculations unless otherwise denoted). We used the GAMESS[50–75] and ACESIII[43] software packages for performing MBPT(2)/ROHF and MBPT(2)/UHF geometry optimizations and hessians, respectively. Analytic force constants were calculated at each step in order to converge to the transition state. Structures were deemed to be converged when the maximum RMS force on any geometric parameter was no greater than 3.3 x 10^{-4} Hartree/Bohr and the total RMS force was no greater than 1.0 x 10^{-4} Hartree/Bohr. On occasion, this protocol produced a structure with a small imaginary frequency between 10 and 20 cm^{-1}; when this happened, the structure was re-optimized with an even tighter protocol until no imaginary frequencies existed larger than 10 cm^{-1} (except for the vibrational mode characterizing the transition state). All coupled cluster energy calculations were performed using the ACESIII program, giving MBPT(2), CCSD, and CCSD(T) energies with the cc-pVTZ and cc-pVQZ basis sets[76]. All core functions were dropped; spherical *d* functions were used in all cases. All reference determinants were converged to 10^{-6} change in density matrix elements; the coupled cluster equations were held to the same convergence criterion for amplitudes. The Helgaker[42] complete basis set extrapolation scheme was also used, although we acknowledge that this extrapolates to the valence basis limit in the absence of core polarization and diffuse functions. Barriers are calculated in the context of Eyring transition state theory. Coordinate information for all intermediates and transition states are in the Supporting Information.

RDX Conformer/Isomer Energetics

Optimized geometries, electronic energies, and estimates of the enthalpy and free energy were obtained for a series of standard RDX conformers with nitro substituents in axial and/or equatorial locations[3] (Table 1) as well as two isomeric structures proposed as reaction intermediates (Fig. 2).[40] The electronic energies of the cyclooctane and NONO isomers were computed to be 19.9 kcal/mol and 16.2 kcal/mol higher in electronic energy, respectively, than the standard RDX conformations. As these are much higher in energy than the standard RDX conformers, and so we did not continue with cc-pVQZ extrapolation given the absence of evidence for a low isomerization barrier, as suggested previously by Bernstein *et al.*[31,35,34] for the degradation mechanism. Electronic energies of the RDX conformers were computed using MBPT(2), CCSD, and CCSD(T) to analyse the degree of convergence (Table 1). These result suggest that the CCSD(T) energy is converged. Enthalpies and Gibbs energies for each of the conformers were then calculated at 298K using CCSD(T) electronic energies, which are superior to CCSD or MBPT(2) values, and MBPT(2) partition functions to obtain the entropy term. Accounting for thermal effects via the enthalpy and Gibbs energies does not alter the relative populations of each conformer to any significant extent.

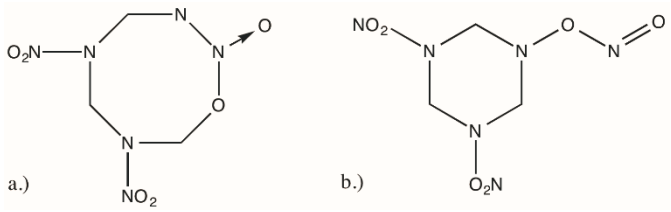

Fig. 2: Structure of the (a) cyclooctane and (b) NONO RDX isomers.

Table 1: Electronic energies (ΔE), enthalpies (ΔH), and Gibbs energies (ΔG) of RDX conformers (kcal/mol). The enthalpy and Gibbs energies are computed using MBPT(2)/cc-pVTZ partition functions and CCSD(T)/CBS electronic energies. We list energies to 0.1 kcal/mol for ease of comparison. Our chosen zero-energy reference state was the most stable conformer in each case.

Many-Body Method	AAA	AAE	AEE	EEE	Boat
ΔE MBPT(2)/TZ	1.3	0.3	1.8	6.7	0
ΔE CCSD/TZ	2.9	0	0.5	5.0	0.3
ΔE CCSD(T)/TZ	1.1	0	1.1	5.8	0.1
ΔE CCSD(T)/QZ	1.3	0	1.1	5.7	0.0
ΔE CCSD(T)/CBS	1.5	0	1.1	5.6	-0.1
ΔH	1.3	0	1.2	5.6	0.1
ΔG	0.8	0	1.1	5.2	0.9

We also determined the transition state for an equatorial/axial transition (AAE→AEE), and calculated a value of 2.0 kcal/mol for the Gibbs energy barrier to inter-conversion. This is in agreement with experimental observations, which yield an estimate of 1.5-5.0 kcal/mol.[77]

Modelling the Initial Steps in RDX Decomposition

NN Homolysis: Previous studies, employing DFT calculations, estimated the barrier to N-N homolysis by considering the relative energies of RDX and the initial products of this reaction.[39] After some effort, however, we were able to locate the first well-characterized transition state structure for NN-homolysis, in which the N-N bond has a length of 2.66 Å (Fig. 3). The difficulty in transition state location was due to the HONO elimination pathway being, effectively, "close." The NN homolysis pathway is the HONO pathway but not stabilized by hydrogen bonding from the methylene CH_2 to the oxygen of the parting NO_2 group (see Fig.3). This chemical insight explains why one might (correctly) guess the barrier to NN homolysis is higher than for HONO elimination. Optimization of the NN homolysis transition state readily moves to the HONO transition state unless one uses a very small trust radius in the geometry optimization. The tendency to jump "too far" is readily accommodated by how close, on the PES, the two pathways are.

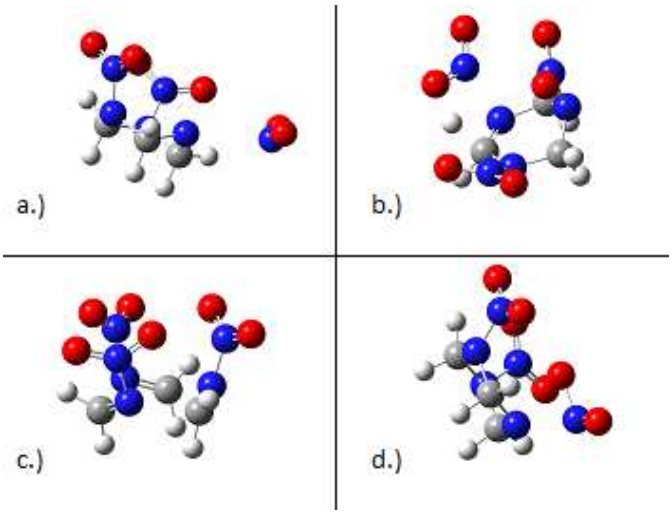

Fig. 3: Molecular Structures of Transition States. a.) NN homolysis, characterized by a 2.66 Å N-N bond. b.) HONO elimination, characterized by a 1.94 Å N-N bond. c.) Triple whammy mechanism, characterized by a 1.44 Å N-N bond. D.) NONO isomerization, characterized by a 1.77 Å N-N bond.

All single-reference coupled cluster methods, however, are sensitive to static correlation, but the inclusion of perturbative triples overcomes many multi-reference (MR) problems.[78] Given the distance of the N-N bond in the TS, we therefore performed an unrestricted reference MBPT(2) optimization; an unrestricted reference may be wiser given the bond-breaking nature. The results differed by less than a kcal/mol in the subsequent electronic energy calculation. The fact that the CCSD(T) energy calculation using either the restricted or unrestricted geometry gives the same result implies that there is minimal static correlation error. In addition, geometry optimization was performed using an aug-cc-pVDZ in addition to the cc-pVTZ basis that we routinely use in our calculations. No dependence on diffuse functions was observed for the

geometry optimization based on the trivially small difference in electronic energy of the two calculated TS structures (approx. 1 kcal/mol). Admittedly, it could be a coincidence that a reduction in the number of high angular momentum functions in favour of more diffuse functions resulted in approximately the same energy.

Table 2: Electronic energies ($\Delta E^{\ddagger}$), enthalpies ($\Delta H^{\ddagger}$), and Gibbs energies ($\Delta G^{\ddagger}$) of the barrier for NN homolysis (kcal/mol) (Fig. 1a). The enthalpy and Gibbs energies are computed using MBPT(2)/cc-pVTZ partition functions and CCSD(T)/CBS electronic energies. We list energies to 0.1 kcal/mol for ease of comparison.

MP2/aug-cc-pVDZ Optimization	AAA	AAE	MP2/cc-pVTZ Optimization	AAA	AAE
$\Delta E^{\ddagger}$ MBPT(2)	49.2	50.1	$\Delta E^{\ddagger}$ MBPT(2)	48.7	49.7
$\Delta E^{\ddagger}$ CCSD	81.9	84.8	$\Delta E^{\ddagger}$ CCSD	78.0	80.9
$\Delta E^{\ddagger}$ CCSD(T)/TZ	55.9	57.0	$\Delta E^{\ddagger}$ CCSD(T)	55.2	56.3
$\Delta E^{\ddagger}$ CCSD(T)/QZ			$\Delta E^{\ddagger}$ CCSD(T)/QZ	56.6	57.9
$\Delta E^{\ddagger}$ CCSD(T)/CBS			$\Delta E^{\ddagger}$ CCSD(T)/CBS	57.7	59.1
			$\Delta E^{\ddagger}$ B3LYP/ 6-311+G**[35]	38.9	
			$\Delta E^{\ddagger}$ B3LYP/ 6-31G*[34]	39.0	
$\Delta H^{\ddagger}$ CCSD(T)	53.7	54.7	$\Delta H^{\ddagger}$ CCSD(T)	56.7	58.0
$\Delta G^{\ddagger}$ CCSD(T)	51.3	51.7	$\Delta G^{\ddagger}$ CCSD(T)	53.9	54.7

We found no clear convergence of electronic energies in going from MBPT(2) to CCSD(T) (Table 2), with the CCSD and CCSD(T) estimates being very different even though the MBPT(2) and CCSD(T) energies were similar. We view the agreement between MBPT(2) and CCSD(T) as coincidence. This difficulty in convergence of many-body excitations is consistent with a description of *partially* delocalized electrons from homolytic cleavage to couple and thereby produce multi-reference effects (over a bond length distance of 2.66Å. Not only does such a hypothesis explain the very different CCSD and CCSD(T) estimates of the barrier, but also differences in our electronic energy barriers and those obtained in prior B3LYP DFT calculations. Thus, previous computational estimates gauged the barrier to be 38.9 kcal/mol[39]; another estimate for this barrier, which was based on comparing adiabatic bond stretching using DFT, gave 39.0 kcal/mol[38]. These DFT-based values are 18 kcal/mol lower than the barrier calculated by CCSD(T) (Table 1). When one considers the more realistic enthalpy and Gibbs energy barriers, our computed barrier is decreased but is still larger than prior estimates by over 10 kcal/mol. In case the inclusion of diffuse functions affects our estimates, we computed the barrier using CCSD(T)/aug-cc-pVTZ to obtain the electronic energy estimates. These calculations increased the barrier by 1.4 kcal/mol. Comparing calculated and experimental values is complicated by the wide range of values (30-50 kcal/mol)[1] that have been reported for the Arrhenius activation energy in the literature. However, if NN homolysis were the dominant mechanism, only the upper estimates would be consistent with our calculated activation enthalpy.

The energetics of RDR, the NN homolysis decomposition product, are available in the SI.

HONO Elimination: The transition state located for the HONO elimination pathway has a nitro group adopting a position intermediate between axial and equatorial (termed the "pseudo" position in the literature[14]). The barriers for HONO elimination were computed separately for the AAA, AAE, and AEE conformers of RDX (Table 3) given that one nitramine adopted an axial position in our calculated TS (Fig.3) HONO elimination from the AEE conformer gives the smallest free energy barrier, and the transition state electronic energy is converged given that the MBPT(2), CCSD, and CCSD(T) values are very similar (Table 3). Our benchmark value of 45.9 kcal/mol for the electronic energy differs from previous DFT estimates of 42.4 kcal/mol and 39.2 reported by Miao *et al.*[39] and Chakraborty *et al.,*[38] respectively. The Miao *et al.* value is off by 3.5 kcal/mol in the electronic energy barrier. The importance of considering thermal effects is also evident from the calculations because the barrier to HONO elimination for the AEE conformer is reduced by 4.4 kcal/mol to 41.9 kcal/mol when they are included. Given that our calculated free energy barrier for NN-homolysis is 53.9 kcal/mol, our results suggest that HONO elimination is the dominant mechanism of gas-phase RDX decomposition at standard temperature and pressure (STP).

Table 3: Electronic energies ($\Delta E^{\ddagger}$), enthalpies ($\Delta H^{\ddagger}$), and Gibbs energies ($\Delta G^{\ddagger}$) of the barrier for HONO elimination (kcal/mol) (Fig. 1b). The enthalpy and Gibbs energies are computed using MBPT(2)/cc-pVTZ partition functions and CCSD(T)/CBS electronic energies. We list energies to 0.1 kcal/mol for ease of comparison.

Many-Body Method	AAA	AAE	AEE
$\Delta E^{\ddagger}$ MBPT(2)	44.8	45.8	44.3
$\Delta E^{\ddagger}$CCSD	50.5	53.4	52.9
$\Delta E^{\ddagger}$ CCSD(T)/TZ	44.8	45.9	44.9
$\Delta E^{\ddagger}$ CCSD(T)/QZ	45.5	46.8	45.7
$\Delta E^{\ddagger}$ CCSD(T)/CBS	45.9	47.4	46.3
$\Delta E^{\ddagger}$ B3LYP/ 6-311+G**[35]	39.2		
$\Delta E^{\ddagger}$ B3LYP/ 6-31G*[34]	42.4		
$\Delta H^{\ddagger}$ CCSD(T)	40.9	42.2	41.0
$\Delta G^{\ddagger}$ CCSD(T)	42.2	43.0	41.9

Triple Whammy: The "triple whammy" mechanism features a complicated transition state, with *potentially* high levels of static correlation (3 bonds are being broken at once) and dynamic correlation. In our "late" TS for this mechanism (Fig. 3), however, the products are nearly formed, resulting in relatively little static correlation. In addition, the transition state is C_3 symmetric with all the nitramine groups in an axial orientation, and thus only relatable to the AAA conformer of RDX. Efforts to find the transition state for other possible rotamers (EEE, AAE and AEE) failed. The lateness of the transition state means that there is very little static but high dynamic correlation. Given that the MBPT(2), CCSD, and CCSD(T) energies are all close, the differences in the electronic energy barriers computed from CCSD and CCSD(T) correspond purely to capturing the intermolecular forces in this late TS.

Our electronic barrier of 68.2 kcal/mol differs from previous estimates, which were reported to be 59.4 kcal/mol and 63.0 kcal/mol on the basis of B3LYP/6-31G(d)[38] and B3LYP/6-311+G(d,p)[39] calculations, respectively. These differences are likely attributable to the inability of the B3LYP functional to describe intermolecular forces. The free energy barrier computed for the "triple whammy" transition state (Table 4), even accounting for entropic effects that lower the barrier, is substantially higher than those calculated for NN homolysis (Table 2).

Table 4: Electronic energies ($\Delta E^{\ddagger}$), enthalpies ($\Delta H^{\ddagger}$), and Gibbs energies ($\Delta G^{\ddagger}$) of the barrier for the "triple whammy" mechanism (kcal/mol) (Fig. 1c). The enthalpy and Gibbs energies are computed using MBPT(2)/cc-pVTZ partition functions and CCSD(T)/CBS electronic energies. We list energies to 0.1 kcal/mol for ease of comparison.

Many-Body Method	AAA
$\Delta E^{\ddagger}$ MBPT(2)	73.4
$\Delta E^{\ddagger}$ CCSD	72.9
$\Delta E^{\ddagger}$ CCSD(T)/TZ	67.2
$\Delta E^{\ddagger}$ CCSD(T)/QZ	67.8
$\Delta E^{\ddagger}$ CCSD(T)/CBS	68.2
$\Delta E^{\ddagger}$ B3LYP/ 6-311+G**[34]	63.0
$\Delta E^{\ddagger}$ B3LYP/ 6-31G*[35]	59.4
$\Delta H^{\ddagger}$ CCSD(T)	63.9
$\Delta G^{\ddagger}$CCSD(T)	62.4

NONO Isomerization: The NONO isomerization decomposition pathway consists of isomerization followed by cleavage of the newly formed ON bond (Table 5). A transition state for the isomerization step was located (Fig. 3), in which two nitro groups occupied axial orientations, suggesting that reaction proceeded from either the AAE or AAA conformer.

Table 5: Electronic energies ($\Delta E^{\ddagger}$), enthalpies ($\Delta H^{\ddagger}$), and Gibbs energies ($\Delta G^{\ddagger}$) of the barriers for NONO isomerization and subsequent ON bond homolysis (kcal/mol) (Fig. 1d). The enthalpy and Gibbs energies are computed using MBPT(2)/cc-pVTZ partition functions and CCSD(T)/CBS electronic energies. We list energies to 0.1 kcal/mol for ease of comparison.

NONO Isomerization	AAE	NONO Cleavage	NONO Intermediate
$\Delta E^{\ddagger}$ MBPT(2)	87.7	$\Delta E^{\ddagger}$ MBPT(2)	8.0
$\Delta E^{\ddagger}$ CCSD	90.7	$\Delta E^{\ddagger}$ CCSD	7.3
$\Delta E^{\ddagger}$ CCSD(T)/TZ	81.3	$\Delta E^{\ddagger}$ CCSD(T)/TZ	7.2
$\Delta E^{\ddagger}$ CCSD(T)/QZ	81.7	$\Delta E^{\ddagger}$ CCSD(T)/QZ	7.2
$\Delta E^{\ddagger}$ CCSD(T)/CBS	82.0	$\Delta E^{\ddagger}$ CCSD(T)/CBS	7.2
$\Delta H^{\ddagger}$ CCSD(T)	80.8	$\Delta H^{\ddagger}$ CCSD(T)	3.1
$\Delta G^{\ddagger}$ CCSD(T)	81.3	$\Delta G^{\ddagger}$ CCSD(T)	0.1

The energetic barriers to isomerization are again very high, making it is unlikely that the NONO isomerization pathway would contribute significantly to gas-phase RDX decomposition. Given the extremely high barriers for AAE, we do not list AAA barriers. Our high barrier sharply contrasts, however, with prior claims by Guo *et al.*[31] who reported an electronic energy barrier to isomerization in the EEE conformer of only 22.6 kcal/mol based on MBPT(2)/6-31G(d) structures/energies. The basis for this large discrepancy remains to be determined given that no geometric information is readily available for the isomerization transition state obtained in the study of Guo *et al.*[31]. Independent of the isomerization step, it is clear that the electronic energy barrier for ON bond cleavage is small and that this reaction is thermally accessible (Table 5).

Modelling Subsequent Steps in the HONO Elimination Pathway

These calculations on the barriers to the initial step of gas-phase RDX decomposition, using CCSD(T)/CBS electronic energies and MBPT(2)/cc-pVTZ-based partition functions, suggest that HONO elimination is energetically preferred, in agreement with the findings of Chakraborty *et al.*[38] This finding is also consistent with experimental activation energy (see below) and kinetic isotope effect[79] measurements of HMX. However, a smaller barrier for a first step leading to subsequent steps with high barriers is ultimately irrelevant. We thus investigate the free energy barriers for steps that might take place **after** formation of the initial intermediate (reactant, Fig. 4): a *first* NN homolysis, a *second* HONO elimination, or a C-N bond scission to cleave the ring.

NN Homolysis: Given that the radical **2** formed by NN homolysis in the initial intermediate **1** could be resonance stabilized (Fig. 4), we anticipated that the barrier for this reaction would be smaller than that calculated for RDX itself.

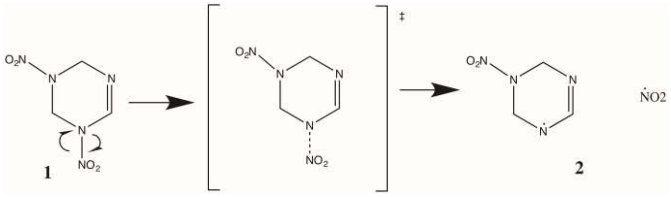

Fig. 4: NN homolysis in intermediate **1** formed by HONO elimination in RDX.

As in our earlier studies, we observed that the CCSD estimate of the electronic energy for the TS was much higher than that obtained in CCSD(T) calculations (Table 6); this is again consistent with the idea that the partially localized electrons couple, thereby resulting multi-reference effects. We are

Table 6: Electronic energies ($\Delta E^{\ddagger}$), enthalpies ($\Delta H^{\ddagger}$), and Gibbs energies ($\Delta G^{\ddagger}$) of the barrier for NN homolysis in intermediate **1** (kcal/mol) (Fig. 4). The enthalpy and Gibbs energies are computed using MBPT(2)/cc-pVTZ partition functions and CCSD(T)/CBS electronic energies. We list energies to 0.1 kcal/mol for ease of comparison.

Many-Body Method	Barrier
$\Delta E^{\ddagger}$ MBPT(2)	41.2
$\Delta E^{\ddagger}$ CCSD	71.4
$\Delta E^{\ddagger}$CCSD(T)/TZ	46.5
$\Delta E^{\ddagger}$CCSD(T)/QZ	48.6
$\Delta E^{\ddagger}$CCSD(T)/CBS	50.1
$\Delta H^{\ddagger}$ CCSD(T)	48.4
$\Delta G^{\ddagger}$ CCSD(T)	44.7

Table 7: Electronic energies ($\Delta E^{\ddagger}$), enthalpies ($\Delta H^{\ddagger}$), and Gibbs energies ($\Delta G^{\ddagger}$) of the barrier for the second HONO elimination step (kcal/mol) (Fig. 5). The enthalpy and Gibbs energies are computed using MBPT(2)/cc-pVTZ partition functions and CCSD(T)/CBS electronic energies. We list energies to 0.1 kcal/mol for ease of comparison.

Second HONO Elimination		Third HONO Elimination	
$\Delta E^{\ddagger}$ MBPT(2)	44.6	$\Delta E^{\ddagger}$MBPT(2)	36.1
$\Delta E^{\ddagger}$ CCSD	51.6	$\Delta E^{\ddagger}$ CCSD	50.3
$\Delta E^{\ddagger}$CCSD(T)/TZ	44.3	$\Delta E^{\ddagger}$ CCSD(T)/TZ	41.2
$\Delta E^{\ddagger}$CCSD(T)/QZ	45.5	$\Delta E^{\ddagger}$CCSD(T)/QZ	42.4
$\Delta E^{\ddagger}$CCSD(T)/CBS	46.4	$\Delta E^{\ddagger}$CCSD(T)/CBS	43.3
$\Delta H^{\ddagger}$ CCSD(T)	41.3	$\Delta H^{\ddagger}$ CCSD(T)	38.2
$\Delta G^{\ddagger}$ CCSD(T)	41.8	$\Delta G^{\ddagger}$ CCSD(T)	38.6

therefore not assured of convergence in our electronic energy estimate. As expected, however, the barrier for NN homolysis in the intermediate **1** is lowered to 44.7 kcal/mol, which is similar to that for HONO elimination in the initial decomposition step. It is therefore possible that experimental observations of a dependence on $[NO_2]$ for the rate of chemical reaction arise from this process, which takes place *after* an initial HONO elimination. The fact that the barrier for NN homolysis in intermediate **1** is about the same as that for the initial HONO elimination itself might explain why experimental studies detect the products of NN homolysis even though our calculations suggest that this is not the initial decomposition step.

HONO Elimination: Similarly, a second HONO elimination in intermediate **1** to yield a conjugated diene was anticipated to proceed with a lower free energy barrier than for the initial step (Fig. 5). This prediction, however, is not supported by calculation with the electronic energy barrier (41.8 kcal/mol) is trivially different from that computed for the initial HONO elimination (Table 7). In a similar manner, the free energy barrier to a third HONO elimination yielding the aromatic heterocycle TAZ[38] (Fig. 6) was determined to be lowered by only 3 kcal/mol relative to that for the initial HONO elimination step (Table 7). Given that all three steps are similar in magnitude, this pathway to TAZ appears kinetically viable.

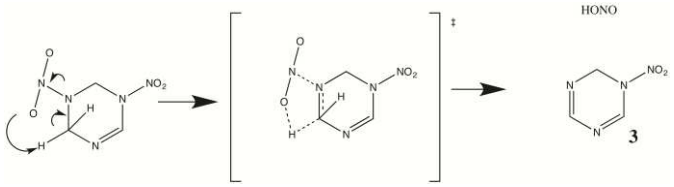

Fig. 5: HONO elimination to form intermediate **3**.

Further degradation of TAZ, however, relies on overcoming the aromatic character of the compound. Indeed, B3LYP/6-31G* calculations by Chakraborty *et al.*[38] gave a large barrier for a "triple whammy" mechanism of TAZ breakdown (Fig. 6) leading to three molecules of HCN. This result is consistent with the free energy barrier of 81.6 kcal/mol obtained using our computational strategy (Table 8). The release of three gaseous particles drastically lowers the product free energies compared to the product electronic energies, emphasizing the importance of including thermal effects. It therefore seems unlikely that this decomposition pathway takes place.

Equally, the "triple whammy" decomposition mechanism of a TAZ precursor (Fig. 7) (formed by two HONO elimination reactions) was investigated by Chakraborty *et al.*[38] and found to have large energy barriers on the basis of B3LYP/6-31G* calculations. Their calculations therefore give the correct qualitative conclusion because calculations using our *ab initio* strategy give a value of 60.3 kcal/mol for the free energy barrier to this concerted reaction (Table 9).

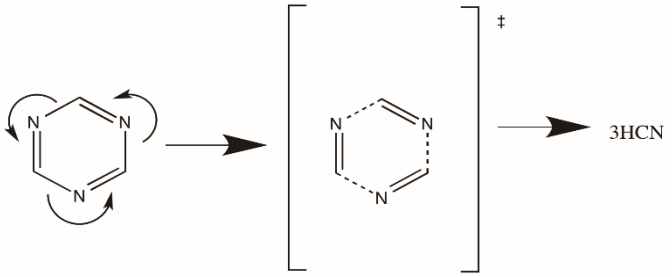

Fig. 6: "Triple whammy" mechanism for TAZ decomposition into hydrogen cyanide

Table 8: Electronic energies ($\Delta E^{\ddagger}$), enthalpies ($\Delta H^{\ddagger}$), and Gibbs energies ($\Delta G^{\ddagger}$) of the barrier for the "triple whammy" decomposition of TAZ (kcal/mol) (Fig. 6). The enthalpy and Gibbs energies are computed using MBPT(2)/cc-pVTZ partition functions and CCSD(T)/CBS electronic energies. We list energies to 0.1 kcal/mol for ease of comparison.

$\Delta E^{\ddagger}$MBPT(2)	86.0
$\Delta E^{\ddagger}$ CCSD	95.0
$\Delta E^{\ddagger}$ CCSD(T)/TZ	88.2
$\Delta E^{\ddagger}$ CCSD(T)/QZ	89.2
$\Delta E^{\ddagger}$ CCSD(T)/CBS	89.9
$\Delta H^{\ddagger}$ CCSD(T)	84.3
$\Delta G^{\ddagger}$ CCSD(T)	81.6

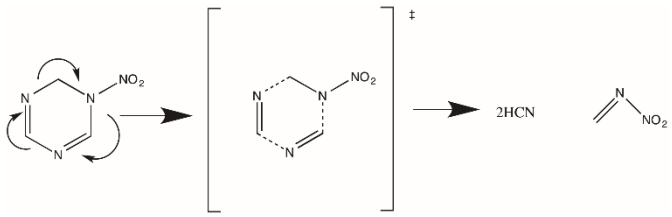

Fig. 7: "Triple whammy" decomposition of intermediate **3**.

Table 9: Electronic energies ($\Delta E^{\ddagger}$), enthalpies ($\Delta H^{\ddagger}$), and Gibbs energies ($\Delta G^{\ddagger}$) of the barrier for a "triple whammy" decomposition of intermediate **3** (kcal/mol) (Fig. 7). The enthalpy and Gibbs energies are computed using MBPT(2)/cc-pVTZ partition functions and CCSD(T)/CBS electronic energies. We list energies to 0.1 kcal/mol for ease of comparison.

$\Delta E^{\ddagger}$ MBPT(2)	64.0
$\Delta E^{\ddagger}$ CCSD	71.1
$\Delta E^{\ddagger}$ CCSD(T)/TZ	66.3
$\Delta E^{\ddagger}$ CCSD(T)/QZ	66.3
$\Delta E^{\ddagger}$ CCSD(T)/CBS	66.4
$\Delta H^{\ddagger}$CCSD(T)	61.7
$\Delta G^{\ddagger}$CCSD(T)	60.3

Faced with these findings, which seem to suggest that a second and third subsequent HONO eliminations lead to intermediates that cannot break down by concerted mechanisms, we have investigated other possible decomposition pathways. For example, we consider NN homolysis of intermediate **3** (Fig. 5) leading to the production of an NO_2 radical (Fig. 8) with a calculated free energy barrier of only 42.8 kcal/mol (Table 10). Given that this value is comparable to that computed for the initial elimination of HONO from RDX, this pathway does appear viable. Once again, we note that MBPT(2) is closer to CCSD(T) than CCSD for the activation energy barrier for an NN homolysis step.

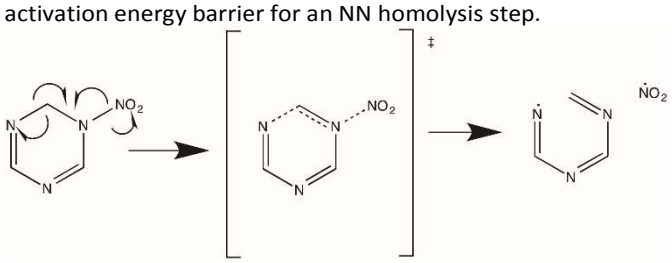

Fig. 8: Ring scission with concomitant NN homolysis in intermediate **3**.

Not only does NN homolysis in this intermediate provide a kinetically reasonable way to break the RDX ring into fragments after HONO elimination, but it is also consistent with experimental claims that RDX decomposition yields products derived from HONO elimination and NN homolysis pathways.

Table 10: Electronic energies ($\Delta E^{\ddagger}$), enthalpies ($\Delta H^{\ddagger}$), and Gibbs energies ($\Delta G^{\ddagger}$) of the barrier for ring scission with concomitant NN homolysis in intermediate **3** (kcal/mol) (Fig. 8). The enthalpy and Gibbs energies are computed using MBPT(2)/cc-pVTZ partition functions and CCSD(T)/CBS electronic energies. We list energies to 0.1 kcal/mol for ease of comparison.

$\Delta E^{\ddagger}$ MBPT(2)	33.9
$\Delta E^{\ddagger}$ CCSD	69.4
$\Delta E^{\ddagger}$ CCSD(T)/TZ	44.7
$\Delta E^{\ddagger}$ CCSD(T)/QZ	46.5
$\Delta E^{\ddagger}$ CCSD(T)/CBS	47.8
$\Delta H^{\ddagger}$ CCSD(T)	45.6
$\Delta G^{\ddagger}$ CCSD(T)	42.8

CN Bond Scission: Another alternative for breaking down the intermediate formed by an initial HONO elimination from RDX would be CN bond scission in the ring (Fig. 9) to yield a radical that could, in principle, react via several possible pathways. We calculate a free energy barrier for this process that are slightly higher (46.5 kcal/mol) than the initial HONO elimination or the other secondary proposed mechanisms (subsequent NN homolysis or concomitant NN homolysis with CN scission) (Table 13). We therefore speculate that this bond cleavage reaction is competitive, albeit slightly disfavoured, with other mechanisms.

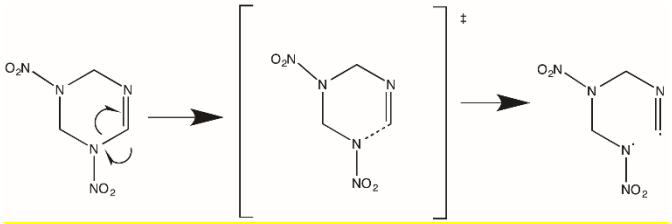

Fig. 9: Ring scission of intermediate **3**.

Table 11: Table 9: Electronic energies ($\Delta E^{\ddagger}$), enthalpies ($\Delta H^{\ddagger}$), and Gibbs energies ($\Delta G^{\ddagger}$) of the barrier for ring scission of intermediate **3** (kcal/mol) (Fig. 9). The enthalpy and Gibbs energies are computed using MBPT(2)/cc-pVTZ partition functions and CCSD(T)/CBS electronic energies. We list energies to 0.1 kcal/mol for ease of comparison.

$\Delta E^{\ddagger}$MBPT(2)	60.8
$\Delta E^{\ddagger}$ CCSD	60.6
$\Delta E^{\ddagger}$CCSD(T)/TZ	58.4
$\Delta E^{\ddagger}$CCSD(T)/QZ	57.2
$\Delta E^{\ddagger}$CCSD(T)/CBS	56.3
$\Delta H^{\ddagger}$ CCSD(T)	50.6
$\Delta G^{\ddagger}$ CCSD(T)	46.5

Comparing CCSD(T) Eyring Barriers with Experimental Kinetics Data

The Arrhenius expression for kinetics describes the rate constant, k, in terms of a pre-exponential factor, A, and an "activation energy," E_a:

$$k=A \exp(-\beta E_a) \quad \text{(Eq. 1)}$$

Similarly, an Eyring model relates the rate constant to thermodynamic quantities, such as the activation free energy components at a given temperature T:

$$k=k_bT/h \exp(-\beta\Delta H^{\ddagger})\exp(\Delta S^{\ddagger}/R) \quad \text{(Eq. 2)}$$

where k_b is the Boltzmann constant, h is Planck's constant and R is the ideal gas constant. Converting our CCSD(T)-derived Eyring barrier for the initial HONO elimination by substituting (1) into (2) yields an E_a value of 41.5 kcal/mol and lnA of 27.5 Hz. Building on the compilation of Brill *et al.*[1], our calculated values of the Arrhenius parameters are in agreement with experimental findings for the RDX decomposition in the gas phase (Table 13).

Table 12: Experimental Arrhenius parameters reported for RDX decomposition.

Phase	E_a kcal/mol	lnA	Ref
Gas	28.6	10.6	[80]
Gas	47.1	42.1	[81]
Gas	47.9	43.1	[82]
Gas	48.7	44.3	[26]
Gas	47 ± 1	42.2	[25]
Gas	34.1	31.1	[27]
Gas	40 ± 3	37 ± 5	[83]
Our Work:	**41.5**	**27.5**	-
Gas	47-53 (range)	18.4-20.8 (range)	[80]
Dilute Solution	38	32.9	[84]

As one can see, however, there is considerable diversity in the experimental values for the gas-phase decomposition of RDX, which may reflect the range of how experimental conditions stimulate decomposition (photons, heat, mechanical) and a wide range of temperatures[1]. The assumptions inherent to our analysis (Eyring TS formalism, harmonic oscillator vibrational partition functions, MBPT(2) geometries) may cause us to under-estimate the barrier or some experimental estimates may be too high. We expect less agreement in the calculated estimate of the pre-exponential factor, lnA, with experiment because this is a function of the activation entropy barrier (in Eyring formalism) and our models for the partition function are based on the harmonic approximation. An accurate calculation of lnA would require anharmonic effects, which is currently non-trivial, computationally. We also note that there is considerable variation in the values of lnA, experimentally; this perhaps owes to the fact that the rigor of an effective collision constant may be lacking. It should also be evident that "the mechanism" even within any one phase is highly variable as a function of pressure and temperature for RDX[85]. This merely serves as a benchmark of accuracy at gaseous STP.

Conclusion

We present here a new analysis of gas phase RDX decomposition pathways using CCSD(T)/CBS methods, often defined as the "gold standard" of quantum chemistry. We find that HONO elimination dominates the initial step of the reaction (with an activation barrier of approximately 40 kcal/mol depending on the ground state conformer) in agreement with the conclusions of Chakraborty *et al.*[38] This value for HONO elimination is consistent with several experimental estimates of the barriers[25,84,86–88], and evidence for a 5-membered ring transition state[28]. Given that the equivalent barrier for NN homolysis in RDX is larger by about 10 kcal/mol, we do not believe that these two pathways compete in the initial step. On this point, we note that this finding is based on the energy of a "true" TS for NN homolysis, which appears to be the first reported in the literature.

Reaction pathways are also proposed to account for what happens after the initial HONO elimination, making sure that their activation free energy barriers are consistent with that for the initial step. Two of these subsequent steps (NN homolysis in the intermediate formed by the initial HONO elimination, or NN homolysis with concomitant ring opening in the intermediate produced by two consecutive HONO eliminations) have sufficiently low barriers as to render them accessible for RDX decomposition. These reactions both release a NO_2 radical, and therefore offer an alternative explanation as to why experiments observe NO_2 concentration to increase with reaction rate, even though calculations do not support NN homolysis as the initial degradation step.

Acknowledgements

We acknowledge the Army Research Office (US. ARO. W911NF-12-1-0143) and the National Science Foundation (CNS-0521433). Computer time was provided by the DoD High Performance Computing Modernization Program at Spirit, Kilrain, and Garnet. Calculations were also performed on Big Red II (Indiana University), which is supported in part by the Lilly Endowment, Inc., through a grant to the IU Pervasive Technology Institute. The Indiana METACyt Initiative at IU is also supported in part by the Lilly Endowment, Inc.

Notes and References

1 T. B. Brill, P. E. Gongwer and G. K. Williams, *J. Phys. Chem.*, 1994, **98**, 12242–12247.
2 W. C. McCrone, *Anal. Chem.*, 1950, **22**, 954–955.
3 R. W. Molt, T. Watson, V. F. Lotrich and R. J. Bartlett, *J. Phys. Chem. A*, 2011, **115**, 884–890.
4 B. M. Rice and C. F. Chabalowski, *J. Phys. Chem. A*, 1997, **101**, 8720–8726.
5 R. J. Karpowicz, S. T. Sergio and T. B. Brill, *Ind. Eng. Chem. Prod. Res. Dev.*, 1983, **22**, 363–365.
6 R. J. Karpowicz and T. B. Brill, *J. Phys. Chem.*, 1984, **88**, 348–352.
7 E. F. C. Byrd, G. E. Scuseria and C. F. Chabalowski, *J. Phys.*

Chem. B, 2004, **108**, 13100–13106.
8 N. Goto, H. Fujihisa, H. Yamawaki, K. Wakabayashi, Y. Nakayama, M. Yoshida and M. Koshi, *J. Phys. Chem. B*, 2006, **110**, 23655–9.
9 E. F. C. Byrd and B. M. Rice, *J. Phys. Chem. C*, 2007, **111**, 2787–2796.
10 J. A. Ciezak, T. A. Jenkins, Z. Liu and R. J. Hemley, *J. Phys. Chem. A*, 2007, **111**, 59–63.
11 D. I. A. Millar, I. D. H. Oswald, C. Barry, D. J. Francis, W. G. Marshall, C. R. Pulham and A. S. Cumming, *Chem. Commun. (Camb).*, 2010, **46**, 5662–4.
12 M. D. Pace, *J. Phys. Chem.*, 1991, **95**, 5858–5864.
13 P. Politzer, J. S. Murray, P. Lane, P. Sjoberg and H. G. Adolph, *Chem. Phys. Lett.*, 1991, **181**, 78–82.
14 R. W. Molt, T. Watson, A. P. Bazanté and R. J. Bartlett, *J. Phys. Chem. A*, 2013, **117**, 3467–3474.
15 R. W. Molt, R. J. Bartlett, T. Watson and A. P. Bazanté, *J. Phys. Chem. A*, 2012, **116**, 12129–12135.
16 H. H. Cady, a. C. Larson and D. T. Cromer, *Acta Crystallogr.*, 1963, **16**, 617–623.
17 C. S. Choi and H. P. Boutin, *Acta Crystallogr. Sect. B Struct. Crystallogr. Cryst. Chem.*, 1970, **26**, 1235–1240.
18 P. Main, R. E. Cobbledick and R. W. H. Small, *Acta Crystallogr.*, 1985, **C41**, 1351–1354.
19 D. C. Sorescu, B. M. Rice and D. L. Thompson, *J. Phys. Chem. B*, 1998, **102**, 948–952.
20 M. F. Foltz, C. L. Coon, F. Garcia and A. L. Nichols, *AD- C049 633L (93-0001), p 9, Apr 92, Contract W-7405-ENG-48, CPIA Abstract No. 93-0003, AD D605 199, U-D; Chemical Propulsion Information Agency: Columbia, MD.*, .
21 N. B. Bolotina, M. J. Hardie, R. L. Speer Jr and A. A. Pinkerton, *J. Appl. Crystallogr.*, 2004, **37**, 808–814.
22 S. Okovytyy, Y. Kholod, M. Qasim, H. Fredrickson and J. Leszczynski, *J. Phys. Chem. A*, 2005, **109**, 2964–70.
23 R. Shaw and F. E. Walker, *J. Phys. Chem.*, 1977, **81**, 2572–2576.
24 J. D. Cosgrove and A. J. Owen, *Chem. Commun.*, 1968, 286.
25 A. J. B. Robertson, *Trans. Faraday Soc.*, 1949, **45**, 85.
26 F. C. Rauch and A. J. Fanelli, *J. Phys. Chem.*, 1969, **73**, 1604–1608.
27 R. N. Rogers and G. W. Daub, *Anal. Chem.*, 1973, **45**, 596–600.
28 H. Zuckermann, G. D. Greenblatt and Y. Haas, *J. Phys. Chem.*, 1987, **91**, 5159–5161.
29 S. Bulusu, D. I. Weinstein, J. R. Autera and R. W. Velicky, *J. Phys. Chem.*, 1986, **90**, 4121–4126.
30 X. Zhao, E. J. Hintsa and Y. T. Lee, *J. Chem. Phys.*, 1988, **88**, 801.
31 Y. Q. Guo, M. Greenfield, A. Bhattacharya and E. R. Bernstein, *J. Chem. Phys.*, 2007, **127**, 154301.
32 T. R. Botcher and C. A. Wight, *J. Phys. Chem.*, 1994, **98**, 5441–5444.
33 S. A. Shackelford, M. B. Coolidge, B. B. Goshgarian, B. A. Loving, R. N. Rogers, J. L. Janney and M. H. Ebinger, *J. Phys. Chem.*, 1985, **89**, 3118–3126.
34 Y. Q. Guo, M. Greenfield and E. R. Bernstein, *J. Chem. Phys.*, 2005, **122**, 244310.
35 H. S. Im and E. R. Bernstein, *J. Chem. Phys.*, 2000, **113**, 7911–7918.
36 C. J. Wu and L. E. Fried, *J. Phys. Chem. A*, 1997, **101**, 8675–8679.
37 N. J. Harris and K. Lammertsma, *J. Am. Chem. Soc.*, 1997, **119**, 6583–6589.
38 D. Chakraborty, R. P. Muller, S. Dasgupta and W. A. Goddard, *J. Phys. Chem. A*, 2000, **104**, 2261–2272.
39 M. Miao, Z. A. Dreger, J. E. Patterson and Y. M. Gupta, *J. Phys. Chem. A*, 2008, **112**, 7383–90.
40 R. J. Bartlett and I. Shavitt, Cambridge University Press, Cambridge U.K., 2009.
41 J. D. Watts, J. Gauss and R. J. Bartlett, *J. Chem. Phys.*, 1993, **98**, 8718.
42 K. L. Bak, P. Jørgensen, J. Olsen, T. Helgaker and W. Klopper, *J. Chem. Phys.*, 2000, **112**, 9229.
43 V. F. Lotrich, N. Flocke, M. Ponton, A. D. Yau, A. S. Perera, E. Deumens and R. J. Bartlett, *J. Chem. Phys.*, 2008, **128**, 194104.
44 K. B. Lipkowitz, D. B. Boyd, R. J. Bartlett and J. F. Stanton, in *Reviews in Computational Chemistry, Volume 5*, eds. K. B. Lipkowitz and D. B. Boyd, John Wiley & Sons, Inc., Hoboken, NJ, USA, 1994, vol. 5, pp. 65–169.
45 M. Urban, J. Noga, S. J. Cole and R. J. Bartlett, *J. Chem. Phys.*, 1985, **83**, 4041.
46 R. J. Bartlett and M. Musial, *Rev. Mod. Phys.*, 2007, **79**, 291–352.
47 F. Coester and H. Kümmel, *Nucl. Phys.*, 1960, **17**, 477–485.
48 R. J. Bartlett and D. M. Silver, *Phys. Rev. A*, 1974, **10**, 1927–1931.
49 T. Helgaker, J. Gauss, P. Jørgensen and J. Olsen, *J. Chem. Phys.*, 1997, **106**, 6430.
50 M. W. Schmidt, K. K. Baldridge, J. A. Boatz, S. T. Elbert, M. S. Gordon, J. H. Jensen, S. Koseki, N. Matsunaga, K. A. Nguyen, S. Su, T. L. Windus, M. Dupuis and J. A. Montgomery, *J. Comput. Chem.*, 1993, **14**, 1347–1363.
51 J. A. Pople and W. J. Hehre, *J. Comput. Phys.*, 1978, **27**, 161–168.
52 B. H. Schlegel, *J. Chem. Phys.*, 1982, **77**, 3676.
53 K. Ishimura and S. Nagase, *Theor. Chem. Acc.*, 2007, **120**, 185–189.
54 L. E. McMurchie and E. R. Davidson, *J. Comput. Phys.*, 1978, **26**, 218–231.
55 H. F. King and M. Dupuis, *J. Comput. Phys.*, 1976, **21**, 144–165.
56 M. Dupuis and H. F. King, *Int. J. Quantum Chem.*, 1977, **11**, 613–625.
57 J. Rys, M. Dupuis and H. F. King, *J. Comput. Chem.*, 1983, **4**, 154–157.
58 G. D. Fletcher, *Int. J. Quantum Chem.*, 2006, **106**, 355–360.
59 M. Dupuis and H. F. King, *J. Chem. Phys.*, 1978, **68**, 3998.
60 T. Takada, M. Dupuis and H. F. King, *J. Chem. Phys.*, 1981, **75**, 332.
61 C. C. J. Roothaan, *Rev. Mod. Phys.*, 1951, **23**, 69–89.
62 J. A. Pople and R. K. Nesbet, *J. Chem. Phys.*, 1954, **22**, 571.
63 J. A. Pople, S. J. Binkley and R. Seeger, *Int. J. Quantum Chem.*, 2009, **10**, 1–19.

64 M. J. Frisch, M. Head-Gordon and J. A. Pople, *Chem. Phys. Lett.*, 1990, **166**, 275–280.
65 T. J. Lee and D. Jayatilaka, *Chem. Phys. Lett.*, 1993, **201**, 1–10.
66 G. D. Fletcher, M. S. Gordon and R. S. Bell, *Theor. Chem. Accounts Theory, Comput. Model. (Theoretica Chim. Acta)*, 2002, **107**, 57–70.
67 C. M. Aikens, G. D. Fletcher, M. W. Schmidt and M. S. Gordon, *J. Chem. Phys.*, 2006, **124**, 14107.
68 J. Baker, *J. Comput. Chem.*, 1986, **7**, 385–395.
69 T. Helgaker, *Chem. Phys. Lett.*, 1991, **182**, 503–510.
70 P. Culot, G. Dive, V. H. Nguyen and J. M. Ghuysen, *Theor. Chim. Acta*, 1992, **82**, 189–205.
71 J. Almlof, K. Faegri and K. Korsell, *J. Comput. Chem.*, 1982, **3**, 385–399.
72 M. Hoser and R. Ahlrichs, *J. Comput. Chem.*, 1989, **10**, 104–111.
73 P. Pulay, *J. Comput. Chem.*, 1982, **3**, 556–560.
74 G. D. Fletcher, M. W. Schmidt, B. M. Bode and M. S. Gordon, *Comput. Phys. Commun.*, 2000, **128**, 190–200.
75 D. G. Fedorov, R. M. Olson, K. Kitaura, M. S. Gordon and S. Koseki, *J. Comput. Chem.*, 2004, **25**, 872–80.
76 T. H. Dunning Jr, *J. Chem. Phys.*, 1989, **90**, 1007.
77 T. Vladimiroff and B. M. Rice, *J. Phys. Chem. A*, 2002, **106**, 10437–10443.
78 A. Perera, R. W. Molt, V. F. Lotrich and R. J. Bartlett, *Theor. Chem. Acc.*, 2014, **133**.
79 S. A. Shackelford, M. B. Coolidge, B. B. Goshgarian, B. A. Loving, R. N. Rogers, J. L. Janney and M. H. Ebinger, *J. Phys. Chem.*, 1985, **89**, 3118–3126.
80 R. N. Rogers and L. C. Smith, *Thermochim. Acta*, 1970, **1**, 1–9.
81 R. N. Rogers, *Thermochim. Acta*, 1974, **9**, 444–446.
82 Y. Oyumi, *Propellants, Explos. Pyrotech.*, 1988, **13**, 42–47.
83 Y. Y. Maksimov, V. N. Apol'kova, O. V. Braverman and A. I. Solov'ev, *Russ. J. Phys. Chem.*, 1985, **59**, 201–204.
84 J. C. Oxley, A. B. Kooh, R. Szekeres and W. Zheng, *J. Phys. Chem.*, 1994, **98**, 7004–7008.
85 I. V. Schweigert, *J. Phys. Chem. A*, 2015, **119**, 2747–2759.
86 G. K. Klimenko, M. S. Belyayeva, L. T. Babaytseva and P. N. Stolyarov, in *5th All-Union Symposium on Cumbustion and Explostion.*, 1977, pp. 47–50.
87 G. K. Klimenko, in *Combustion and Explostion: Materials of the 4th All-Union Symposium on Cumbustion and Explostion.*, Nauka, Moscow, Russia, 1977, pp. 585–593.
88 Y. M. Burov and G. M. Nazin, *Kinet. Catal.*, 1982, **23**, 5–10.

